

A Novel T-type Current Underlies Prolonged Ca^{2+} -dependent Burst Firing in GABAergic Neurons of Rat Thalamic Reticular Nucleus

J. R. Huguenard and D. A. Prince

Department of Neurology and Neurological Sciences, Stanford University Medical Center, Stanford, California 94305

The inhibitory GABAergic projection of thalamic nucleus reticularis (nRt) neurons onto thalamocortical relay cells (TCs) is important in generating the normal thalamocortical rhythmicity of slow wave sleep, and may be a key element in the production of abnormal rhythms associated with absence epilepsy. Both TCs and nRt cells can generate prominent Ca^{2+} -dependent low-threshold spikes, which evoke bursts of Na^+ -dependent fast spikes, and are influential in rhythm generation. Substantial differences in the pattern of burst firing in TCs versus nRt neurons led us to hypothesize that there are distinct forms of transient Ca^{2+} current (I_{T}) underlying burst discharges in these two cell types. Using whole-cell voltage-clamp recordings, we analyzed I_{T} in acutely isolated TCs and nRt neurons and found three key differences in biophysical properties. (1) The transient Ca^{2+} current in nRt neurons inactivated much more slowly than I_{T} in TCs. This slow current is thus termed I_{Ts} . (2) The rate of inactivation for I_{Ts} was nearly voltage independent. (3) Whole-cell I_{Ts} amplitude was increased when Ba^{2+} was substituted for Ca^{2+} as the charge carrier. In addition, activation kinetics were slower for I_{Ts} and the activation range was depolarized compared to that for I_{T} . Other properties of I_{Ts} and I_{T} were similar, including steady-state inactivation and sensitivities to blockade by divalent cations, amiloride, and antiepileptic drugs. Our findings demonstrate that subtypes of transient Ca^{2+} current are present in two different classes of thalamic neurons. The properties of I_{Ts} lead to generation of long-duration calcium-dependent spike bursts in nRt cells. The resultant prolonged periods of GABA release onto TCs would play a critical role in maintaining rhythmicity by inducing TC hyperpolarization and promoting generation of low-threshold calcium spikes within relay nuclei.

Certain oscillatory rhythms within the cerebral cortex are a consequence of both thalamocortical circuitry and intrinsic properties of thalamic neurons (Steriade and Llinás, 1988; Ribary et al., 1991). The thalamus is intimately involved in generation of the rhythmic high-voltage, 7–14 Hz spindles observed in the EEG during certain phases of sleep. Early evidence of this was provided by Morison and Bassett (1945), who showed

that after corticotomy spindle activity could still be recorded in the thalamus. A key element in rhythm generation within the thalamus is the GABAergic nucleus reticularis (nRt) that is reciprocally connected to thalamocortical relay neurons (TCs) of dorsal thalamic nuclei and also receives collateral excitatory connections from corticothalamic fibers (Jones, 1985). Through a series of *in vivo* experiments, Steriade, Deschénes, and colleagues have identified nRt as a key site in the generation of spindle rhythms. During periods of sleep associated with EEG synchronization, spindles are absent in anterior thalamic nuclei that are devoid of connections with nRt (Mulle et al., 1985) and in relay nuclei that have been disconnected from nRt by transection (Steriade et al., 1985). On the other hand, spindles persist in nRt after it has been isolated from other thalamic nuclei (Steriade et al., 1987), when such activity is absent in relay nuclei and in the cortex. These findings implicate the thalamus, and especially nRt, as important rhythm generation sites.

Intrinsic firing properties of nRt cells are an important factor in promoting rhythm generation. Neurons in nRt are characterized by two basic firing patterns (Domich et al., 1986; McCormick and Prince, 1986; Mulle et al., 1986; Steriade et al., 1986; Llinás and Geijo-Barrientos, 1988; Spreafico et al., 1988), similar to those in TCs (Deschénes et al., 1982; Llinás and Jahnsen, 1982). In both cell types, regular repetitive firing is the normal response to excitatory inputs under conditions where the resting membrane potential is relatively depolarized. However, with membrane hyperpolarization, the same inputs produce Ca^{2+} -dependent low-threshold spikes (LTSs) that can trigger several fast Na^+ spikes. In TCs, the LTS is mediated by a transient Ca^{2+} current (T-current, I_{T} ; Coulter et al., 1989a; Crunelli et al., 1989; Hernández-Cruz and Pape, 1989; Suzuki and Rogawski, 1989), and presumably the same or a similar conductance mechanism underlies LTS generation in nRt cells. Since the LTS in nRt is blocked by Cd^{2+} (Avanzini et al., 1989) but persists in the presence of the Na^+ channel blocker QX-314 (Mulle et al., 1986), it is probably mediated by a similar transient Ca^{2+} current. Interestingly, however, the LTSs and burst-firing patterns in nRt cells are fundamentally different from their counterparts in TCs. Extracellular recordings in chronically implanted unanesthetized animals clearly demonstrate that TCs exhibit monophasic spike bursts consisting of 2–10 spikes with an average duration of 8 msec (Domich et al., 1986). In contrast, nRt cells recorded under the same conditions fire bursts consisting of two phases, an early high-frequency “core” burst lasting 50–100 msec, and a late phase of tonic firing that can last for hundreds of milliseconds (Domich et al., 1986; Steriade et al., 1986). While little is known about the mechanisms underlying the tonic firing phase, the core burst is presumably mediated by an LTS. In fact, *in vivo* intracellular recordings reveal that LTSs

Received Jan. 29, 1992; revised Apr. 14, 1992; accepted Apr. 22, 1992.

We thank Richard Tsien and Istvan Mody for helpful discussions and critical reading of the manuscript. Edward Brooks and Isabel Parada provided invaluable technical assistance. This work was supported by NIH Grants NS06477 and NS12151 from the NINDS, and by the Morris and Pimley Research Funds.

Correspondence should be addressed to J. R. Huguenard, Department of Neurology and Neurological Sciences, Room M016, Stanford University Medical Center, Stanford, CA 94305.

Copyright © 1992 Society for Neuroscience 0270-6474/92/123804-14\$05.00/0

in nRt cells are considerably longer than those in TCs (Mulle et al., 1986; Shosaku et al., 1989). Although an extended barrage of EPSPs onto nRt neurons can contribute to elongated LTS bursts under some circumstances, including spindle activity, long bursts also can be induced by intracellular current injection, indicating that nRt cells have intrinsic mechanisms for producing such activity. The prolonged Ca^{2+} -dependent bursts in the GABAergic neurons of nRt presumably evoke either long trains of IPSPs or large IPSPs (due to rapid release of large amounts of GABA) in TCs. In either case, activation of GABA_A receptor-mediated events would be favored since these are thought to require the release of large amounts of GABA (Dutar and Nicoll, 1988). The resulting Cl^- - and K^+ -mediated hyperpolarization, and subsequent deinactivation of I_T , may be a critical factor in rhythm initiation and/or maintenance.

Here we present results of a voltage-clamp study in acutely isolated neurons of rat nRt showing that these cells possess a transient Ca^{2+} current with unique properties. Unlike the transient (low-voltage-activated or T-type) current observed in a number of preparations including relay neurons, I_{Ts} in nRt neurons displays slow and voltage-independent inactivation kinetics. Thus, nRt cells can generate longer-duration LTSs and spike bursts that result in a sustained release of GABA onto TCs.

Portions of these results have been published in preliminary form (Huguenard and Prince, 1991).

Materials and Methods

Tissue slice and isolated cell preparation. Sprague-Dawley rats (postnatal days 7–12) were deeply anesthetized with pentobarbital (50 mg/kg) and decapitated, and the brain was rapidly removed and placed in chilled oxygenated Ringer's solution. Coronal slices with a thickness of 400 μm were then cut on a vibratome. For current-clamp recordings, slices were placed in interface-type chamber and perfused with normal Ringer's solution (see below) equilibrated with 95% O_2 , 5% CO_2 at 34°C.

Neurons of the ventrobasal complex (VB) and nRt were isolated from slices via an enzymatic dissociation procedure that has been previously described (Kay and Wong, 1986; Coulter et al., 1989a). In slices from the most anterior coronal sections containing nRt, the nucleus was relatively wide, and it was possible to resect it from adjacent ventrolateral nucleus and the internal capsule. The nRt sections were crescent shaped rather than rectangular as in VB, but otherwise the dissociation technique was identical for the two nuclei. The voltage-clamp data presented here represent results from 43 nRt and 56 VB neurons.

Histology. For anti-GABA staining of nuclear sections (see Fig. 2*A, B*), the following procedure was used. An 8-d-old rat pup was deeply anesthetized with sodium pentobarbital (50 mg/kg), followed immediately by a transcardiac perfusion with 50 ml of 0.9% NaCl and 200 ml of freshly prepared 4% paraformaldehyde, 0.3% glutaraldehyde in 0.1 M phosphate buffer. The brain was removed and stored overnight at 4°C in the same fixative. The next day, the brain was transferred to PBS and slices of 500 μm were cut using a vibratome. The VB and nRt thalamic nuclei were then dissected from the slices in the same manner in which they are prepared for the dissociation procedure. The tissue was embedded in agar, and serial vibratome sections with a nominal thickness of 50 μm were cut. The sections were then processed for immunocytochemistry using a rabbit anti-GABA serum (Inestar Co.) as follows. Free-floating sections were incubated in 95% EtOH for 3 min, followed by several rinses in PBS, incubation in blocking solution for 1 hr (5% normal goat serum, 0.3% Triton-X in 0.1 M PBS), and finally by incubation in the primary antiserum at a dilution of 1:6000 for 16 hr at 4°C. Sections were then rinsed several times both before and after a 1 hr incubation in the biotinylated secondary antibody. After several rinses in PBS, the sections were incubated for 45 min in the avidin-biotin-peroxidase complex, reacted with diaminobenzidine solution in Tris buffer with 0.002% H_2O_2 , and finally mounted on slides, dried, and coverslipped.

For the isolated cells, the above procedure was slightly modified. Petri dishes containing isolated cells were fixed for 30 min in 4% paraformaldehyde, 0.3% glutaraldehyde, followed by two 10 min rinses in PBS

and then 1 hr of incubation in a blocking solution of 3% normal goat serum, 0.1% Triton-X in PBS. After rinsing in PBS, cells were exposed to the 1° antibody, rat anti-GABA (Inestar; 1:6000), for 12 hr at 4°C, rinsed twice in PBS, and exposed for 45 min to the biotinylated 2° antibody. Following two more rinses in PBS, the tissue was incubated for 45 min in the avidin-biotin-peroxidase complex. Finally the cells were rinsed with 50 mM Tris buffer, incubated with diaminobenzidine solution in Tris buffer with 0.002% H_2O_2 , rinsed again in Tris buffer, and mounted using glycerol.

To identify the neurons in whole-cell recordings from the slice, 0.5% biocytin was included in the intracellular patch pipette solution. Following recording, the slices were immediately fixed and processed using published histochemical procedures (Tseng et al., 1991).

Solutions and drugs. The concentration of solutions used for recording I_{Ca} in isolated cells was (in mM), for intracellular pipette solution, 110 Tris PO₄ dibasic, 28 Tris base, 11 ethyleneglycol-bis-(β -aminoethyl-ether)-N,N,N',N'-tetraacetic acid (EGTA), 2 MgCl₂, 0.5 CaCl₂, 4 Na₂ATP, pH 7.3; and for extracellular solution, 155 tetraethylammonium Cl (TEA), 3 CaCl₂, 10 N-2-hydroxyethylpiperazine-N'-2-ethanesulfonic acid (HEPES), with pH 7.4. Transient Ca^{2+} currents were quite stable under these recording conditions; however, the sustained Ca^{2+} current tended to run down unless an ATP regeneration system (see Forscher and Oxford, 1985) was included in the intracellular solution. This resulted in much more stable sustained Ca^{2+} current amplitude, so it was possible to test reliably for reversible drug-dependent effects on this current as well. In all cases, drug effects were compared to temporally proximate controls to detect any remaining change in currents due to drift or rundown. Drugs were applied via an extracellular perfusion system consisting of an assembly of several parallel tubes (Yellen, 1982) that could be repositioned to effect complete solution changes in less than 1 sec. Chemicals were obtained from Sigma (St. Louis, MO), except ω -conotoxin GVIA (ω -CgTx; Peninsula Labs, Belmont, CA) and dihydropyridines (compliments of Dr Alexander Scriabine, Miles Labs, West Haven, CT). All experiments were performed at room temperature (23–25°C) to promote long-term survival (in some cases, >2 hr) of isolated cells in the recording chamber.

For whole-cell recording in the slice, the following solutions were used (in mM): extracellular Ringer's solution, 122 NaCl, 26 NaHCO₃, 1.2 NaH₂PO₄, 2 MgCl₂, 2 CaCl₂, 3 KCl, 10 glucose; intracellular solution, 135 K-gluconate, 1 MgCl₂, 1 CaCl₂, 11 EGTA, 10 HEPES, pH 7.3.

Data collection and analysis. Current-clamp recordings were obtained via blind whole-cell recordings (Blanton et al., 1989; Otis et al., 1991) in thalamic slices using an Axopatch amplifier. Access resistance was on the order to 10–20 M Ω . For voltage-clamp experiments in isolated cells, whole-cell recordings (Hamill et al., 1981) were obtained with electrodes fabricated from medium-wall borosilicate glass (KG-33, Garner Glass, Claremont, CA). Typical electrode resistance was 5–6 M Ω in the bath, with access resistance in the range of 7–12 M Ω . Recordings were obtained with a List EPC-7 amplifier, and series resistance compensation (\approx 80%) was routinely utilized. Currents were leak subtracted, using a P/4 protocol, and digitally sampled using an INDEC Basic-23 system. Nonlinear simplex routines were used to obtain best-fitted Boltzmann (Eq. 1) and m^2h (Eq. 2) curves. A 9 mV liquid junction potential was subtracted from all command potentials. Cell capacitance was determined by integrating the current response to a 5 mV hyperpolarization and then dividing the resultant charge by the change in voltage.

The voltage protocols that were used for the pharmacological tests (see Figs. 8, 9; Table 2) were designed to isolate T-current and L-current. Depolarizations to -40 mV from a holding potential of -100 mV activate only T-current, since this is below the activation threshold for I_L and I_N (Fox et al., 1987), while depolarizations to +10 mV from a holding potential of -50 mV should activate both I_L and I_N . However, thalamic cells possess little N-current (see Figs. 3, 8, 9; see also Coulter et al., 1989a), and so this protocol activates essentially I_L , since both I_T and I_{Ts} are inactivated at this holding potential (see Fig. 4).

Results

LTSs in TCs and nRt cells

Differences in LTS properties between TCs and nRt neurons in both cat and rat have been described (Mulle et al., 1986; Shosaku et al., 1989). However, it appears from the results of these *in vivo* experiments that variations are due in part to synaptic

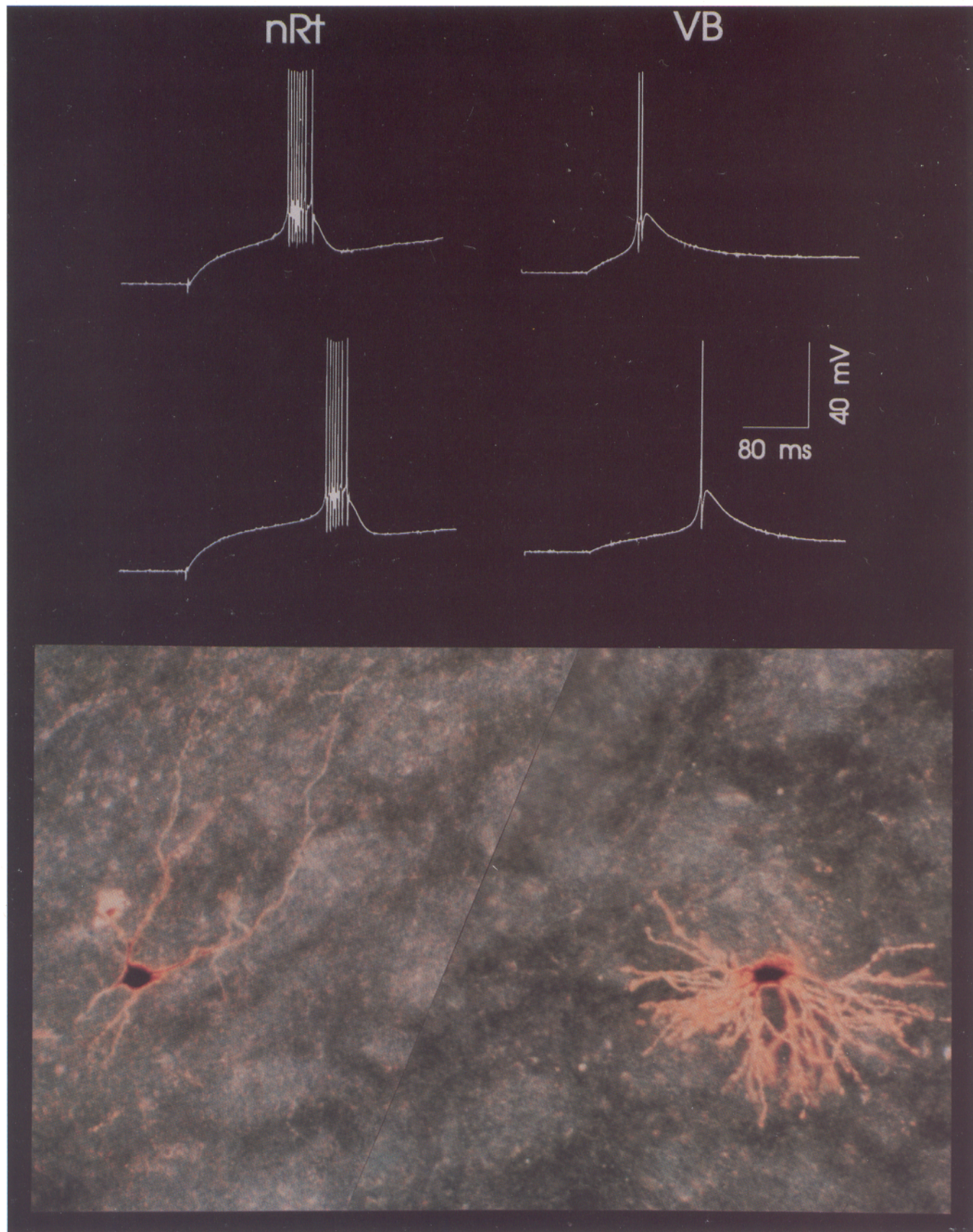


Figure 1. Ca^{2+} -dependent burst responses obtained in representative cells of nRt and VB. *Top*, Voltage recordings obtained with depolarizations from resting potential in representative nRt neurons (*left*; rest = -82 mV; input resistance, $170\text{ M}\Omega$; input capacitance, 69 pF) and VB neurons

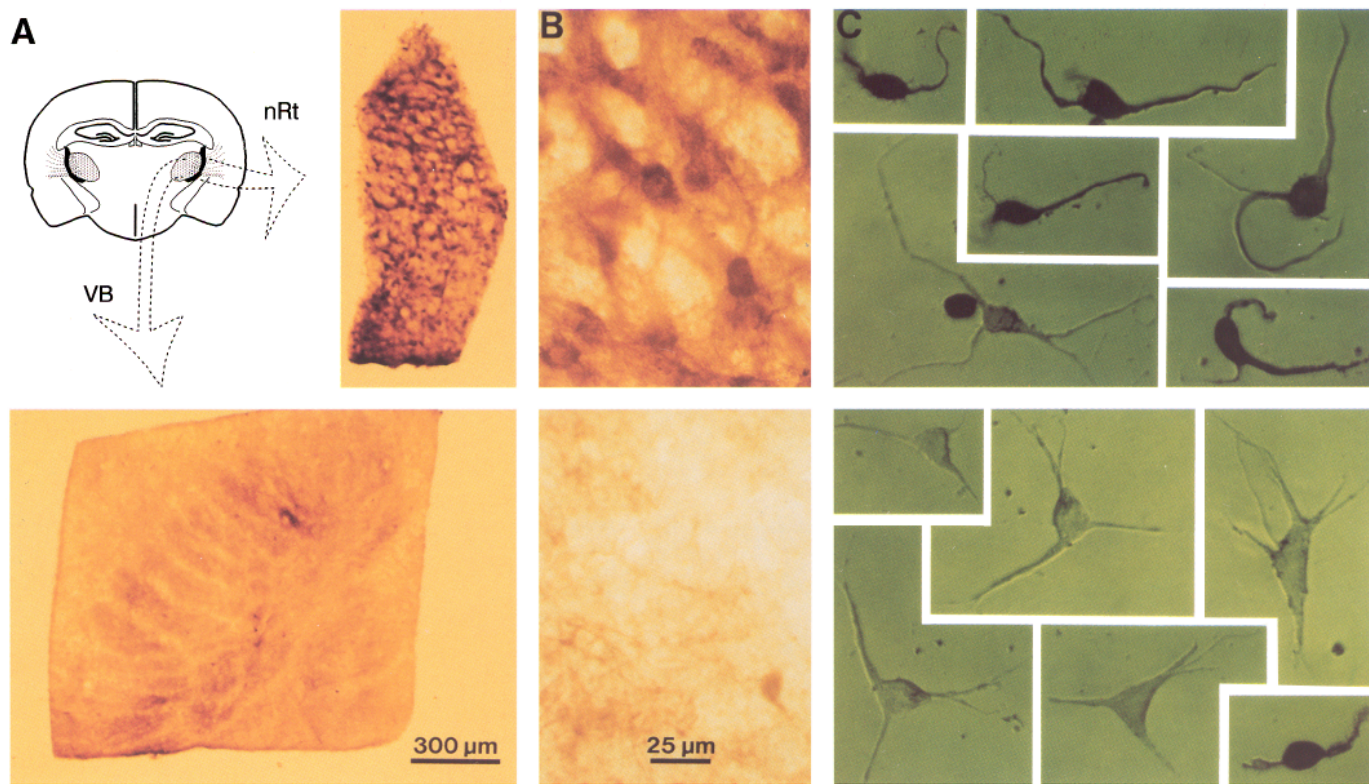


Figure 2. Isolation of VB and nRt neurons from rat. *A*: Top left, Schematic depiction of coronal slice containing both VB (light shading) and nRt (dark shading), and tissue chunks that were stained with an anti-GABA antibody. Top right, Thin crescents were cut from lateral thalamus and carefully trimmed to contain only nRt. In practice, more anterior coronal slices were used to provide wider nRt sections. Darkly staining networks of neurons were observed in nRt. Bottom, VB sections were conservatively trimmed to exclude nRt and then subdivided into cubic sections. These sections contained very few stained somata, but an extensive network of GABAergic fibers and clearly demonstrated barreloids (Jones, 1985). *B*, Higher-magnification images of the sections in *A*. Top, nRt sections contained numerous round, darkly staining somata connected by a network of fibers. Bottom, A small stained cell is seen in the lower right corner, but this section of VB was almost entirely devoid of GABA-positive cells. However, numerous dark-staining fibers are seen. *C*, Isolated neurons obtained from nRt possessed rounded somata, and usually two major dendrites, and were darkly staining. Bottom, VB neurons often had triangular somata and did not stain positively for the presence of GABA. Very occasionally small monopolar or bipolar dark-staining cells were obtained (bottom right).

actions. For example, during rhythmic LTS bursting in rat nRt neurons, membrane hyperpolarization uncovers repetitive excitatory postsynaptic potentials that occur during the rhythmic depolarizations in TCs (Shosaku et al., 1989). In order to compare LTS morphology directly within the two nuclei and to support the suggestion that the some of the differences are dependent on intrinsic membrane properties, we obtained current-clamp recordings in preparations containing both nRt and VB within the same slice. Examples of the LTSs in each cell type are shown in Figure 1. In each cell type, depolarizing intracellular current pulses delivered from the resting potential (-72 to -82 mV) evoked responses consisting of a burst of action potentials riding on a slow underlying LTS. These bursts had distinctive and stereotyped properties. For example, in nRt cells (Fig. 1, top left), the LTS was prolonged so that six or seven high-frequency (>250 Hz) Na^+ spikes were generated at its crest.

In contrast, the LTSs in the relay neurons of VB (Fig. 1, top right) were shorter in duration and evoked only 1 or 2 Na^+ spikes. The remainder of this report focuses on differences in the underlying transient Ca^{2+} currents that contribute to the distinct burst characteristics in these two cell types.

Identification of nRt cells

We compared transient Ca^{2+} current properties of nRt and the prototypical TCs of VB in each animal. Since these nuclei are adjacent, the following measures were used to ensure that isolated cells were derived from the desired nucleus. First, in a few experiments the subdivided nuclear sections were tested for the presence of GABA using standard immunohistochemical procedures. As expected, the tissue chunks isolated from nRt (Fig. 2A, top right) contained many GABA-positive neurons connected via a dense network of darkly staining fibers, more clearly

←

(right; rest = -72 mV; input resistance, $125\text{ M}\Omega$; capacitance, 113 pF). Both cell types exhibit stereotyped burst responses, but nRt bursts contain more spikes that arise from a longer-duration LTS. Recording solution was potassium gluconate with 0.5% (w/v) biocytin. After recording, the slice was processed and visualized with dark-field microscopy and is shown in the photomicrograph at the bottom (magnification, $200\times$). The photomicrograph is a montage of two adjacent sections in register, as necessitated by the fact that the resectioning procedure resulted in the main soma sections of the VB and nRt being located in adjacent $80\text{ }\mu\text{m}$ sections.

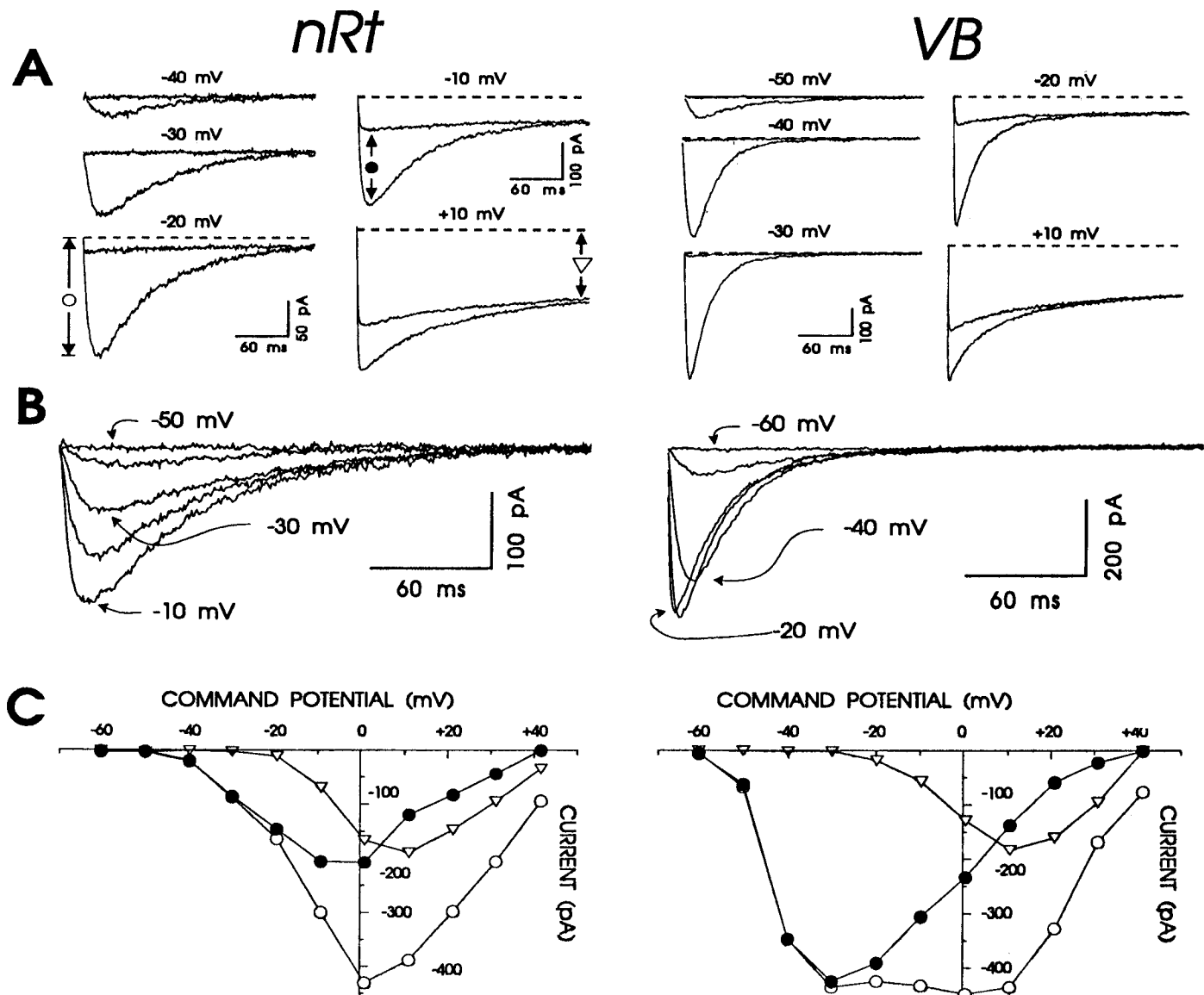


Figure 3. Calcium currents from nRt versus VB neurons. *A*, Currents evoked at the indicated command potentials from holding potentials (V_{hold}) of -100 mV and -50 mV. The larger and more complete inactivating current in each case is that obtained with V_{hold} of -100 mV. *B*, Voltage-inactivated currents. Difference currents obtained for each pair of currents from *A*. In nRt cells, a transient inward current is detectable at -40 mV and becomes larger with stronger depolarizations, but the rate of inactivation is relatively constant. In contrast, the transient current in VB cells is detectable at -50 mV, and the rate of decay becomes faster with increased depolarization. *C*, I - V curves for I_{Ca} . Open circles (\circ) are peak inward current, solid circles (\bullet) are the voltage-inactivated current (as in *B*), and open triangles (∇) are the late noninactivating current obtained with depolarized V_{hold} . The current inactivated by voltage peaks at -30 mV in VB neurons compared to -10 mV in nRt.

seen in Figure 2*B* (top). The round somata in nRt were very darkly stained. In contrast, VB sections contained very few GABA-positive cells (see Jones, 1985; Harris and Hendrickson, 1987); rather, a diffuse projection of fine, darkly staining fibers, which delineated the barreloids (Jones, 1985), was observed in the somatosensory VB (Fig. 2*A*, bottom). GABA-positive cells were rare (Fig. 2*A*, bottom), small, and normally monopolar or bipolar in appearance (e.g., small monopolar cell in the lower right corner of Fig. 2*B*, bottom).

Thalamic neurons could be immunocytochemically identified even after isolation. Cells acutely dissociated from nRt were intensely stained (Fig. 2*C*, top), generally had round somata, and possessed one or two major dendrites. Only rare GABA-positive cells were found in preparations isolated from VB (Fig.

2*C*, bottom right), although small (<2 μm), dark puncta, possibly representing severed terminals from GABAergic nRt cell projections, were observed on the surface of the triangular somata of VB neurons. We were unsuccessful in obtaining unambiguous immunostaining following patch-clamp recordings. However, given the relatively clean separation of nuclei, demonstrated by the above immunohistochemical control experiments, we are confident that the results presented here reflect the properties of two different and relatively homogeneous populations of neurons.

Ca^{2+} currents in nRt versus VB cells

We applied whole-cell clamp techniques to acutely isolated neurons, maintained under conditions where Ca^{2+} currents are se-

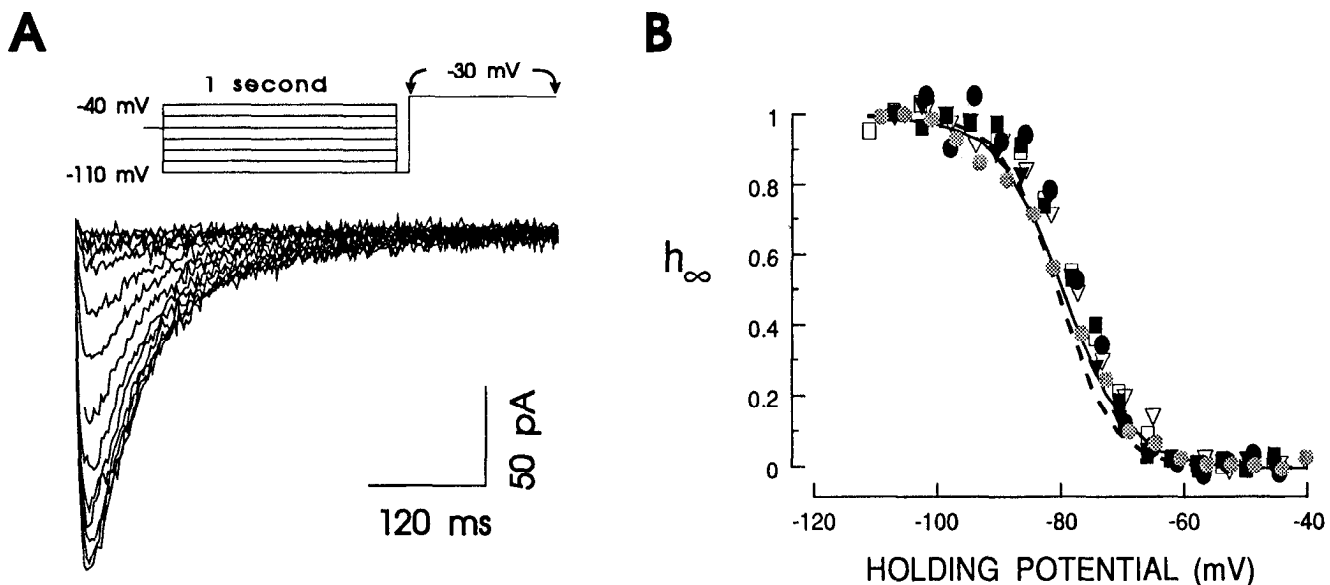


Figure 4. Steady-state inactivation of I_T in nRt cells. *A*, Currents obtained with depolarizations to -30 mV from different holding potentials. At the top, the voltage protocol is depicted: the holding potential was set to the indicated holding potentials for 1 sec, followed by a 10 msec hyperpolarization to -110 mV that preceded the depolarizing command to -30 mV . The traces (bottom) are the currents obtained in the interval between the arrows in the indicated protocol; largest currents were obtained with the most hyperpolarized potentials. *B*, Normalized current amplitude plotted versus holding potential to obtain the h_{∞} curve for six different nRt cells. The shaded circles are from the cell in *A*, and the continuous curve is the best-fitted Boltzmann function with $V_h = -80 \text{ mV}$ and $k = 5.3 \text{ mV}^{-1}$. The discontinuous line is the Boltzmann function describing the average h_{∞} curve for I_T in VB neurons with $V_h = -81 \text{ mV}$ and $k = 4.4 \text{ mV}^{-1}$.

lectively expressed, to determine whether some of the physiological differences between relay neurons and cells of nRt could be due to differences in Ca^{2+} channels. When patch electrodes were filled with Tris-phosphate and the extracellular medium contained TEA with 3 mM CaCl_2 , all voltage-dependent currents evoked between -80 and $+30 \text{ mV}$ were Ca^{2+} dependent as judged by complete blockade with 1 mM extracellular Cd^{2+} or 0.1 mM La^{3+} (see below). The addition of TTX to the bathing solution produced no alteration in Ca^{2+} current, demonstrating that, in contrast to hippocampal neurons (Takahashi et al., 1989), no Ca^{2+} flux occurs through Na^{+} channels in thalamic cells.

In many ways, the inward Ca^{2+} currents of nRt cells were similar to those in TCs. Small depolarizations, in the membrane potential (V_m) range of -30 to -40 mV , evoked rapidly activating Ca^{2+} currents that completely inactivated with maintained depolarization (Fig. 3*A*). There was no detectable current when the same depolarizing commands were applied with the holding potential reduced from -100 mV to -50 mV . Thus, in nRt neurons, as in TCs, I_T is largely inactivated at normal resting potentials. Although a T-type current was present in each cell type, there were significant differences between I_T in nRt cells and TCs. At command potentials of -30 and -40 mV , the I_T was completely inactivated within about 110 msec in VB cells, compared to nearly 220 msec in nRt (Fig. 3*B*). In addition, the rate of I_T inactivation in VB cells was voltage dependent (Coulter et al., 1989a), such that the time constant of current decay became shorter with stronger depolarizations (right traces, Fig. 3*B*). By contrast, the rate of decay of T-current in nRt cells was insensitive to membrane potential. Also, in nRt both the apparent activation threshold (-40 mV ; Fig. 3*C*) and the potential at which the current attained peak amplitude (-10 mV) were more depolarized than in VB cells (-50 mV and -30 mV , respectively). Finally, peak I_T amplitude was larger in VB cells ($280 \pm 23 \text{ pA}$; $n = 26$) than in those of nRt ($131 \pm 15 \text{ pA}$; $n = 23$; two-tailed *t* test, $p < 0.001$). The differences in peak amplitude cannot be accounted for by cell size, since membrane area, as estimated by whole-cell capacitance, was not different between VB and nRt cells ($16.7 \pm 1.1 \text{ pF}$, $n = 21$, vs $17.1 \pm 1.2 \text{ pF}$, $n = 19$, respectively).

In a subpopulation of nRt cells (16 out of 43), the kinetic properties of the transient Ca^{2+} current were indistinguishable from those of I_T as seen in VB cells. It is possible that these results either were from a true subpopulation of nRt cells, or were due to contamination from nearby TCs, resulting from incomplete microdissection. With preparations obtained from the most anterior sections of thalamus, where it was possible to isolate nRt more completely, only cells with the slow T-current were obtained. However, there are anatomical data (Spreafico et al., 1988) that support the existence of more than one subtype of nRt cell. Therefore, it remains a distinct possibility that there is heterogeneity of I_T within nRt. Interestingly, the two forms of I_T were mutually exclusive, that is, within a given cell only one type of transient Ca^{2+} current existed.

Steady-state inactivation of I_{T_s}

There are some similarities between I_{T_s} described here and the N-type current (I_N) as described in sensory neurons (Fox et al., 1987), especially in terms of inactivation rate. However, there are clear distinctions between I_T and I_N regarding the voltage dependencies of both activation and inactivation. I_N is activated by large depolarizations in the range of -20 mV to $+30 \text{ mV}$, whereas I_T is activated between -70 and -30 mV (Fox et al., 1987). On the other hand, I_T is steady-state inactivated between -100 and -60 mV while I_N is inactivated between -100 and -30 mV . In a set of experiments designed to identify and characterize I_{T_s} and differentiate it from I_N , we studied the voltage dependence of activation and inactivation in nRt cells and compared these properties to those of I_T in VB neurons.

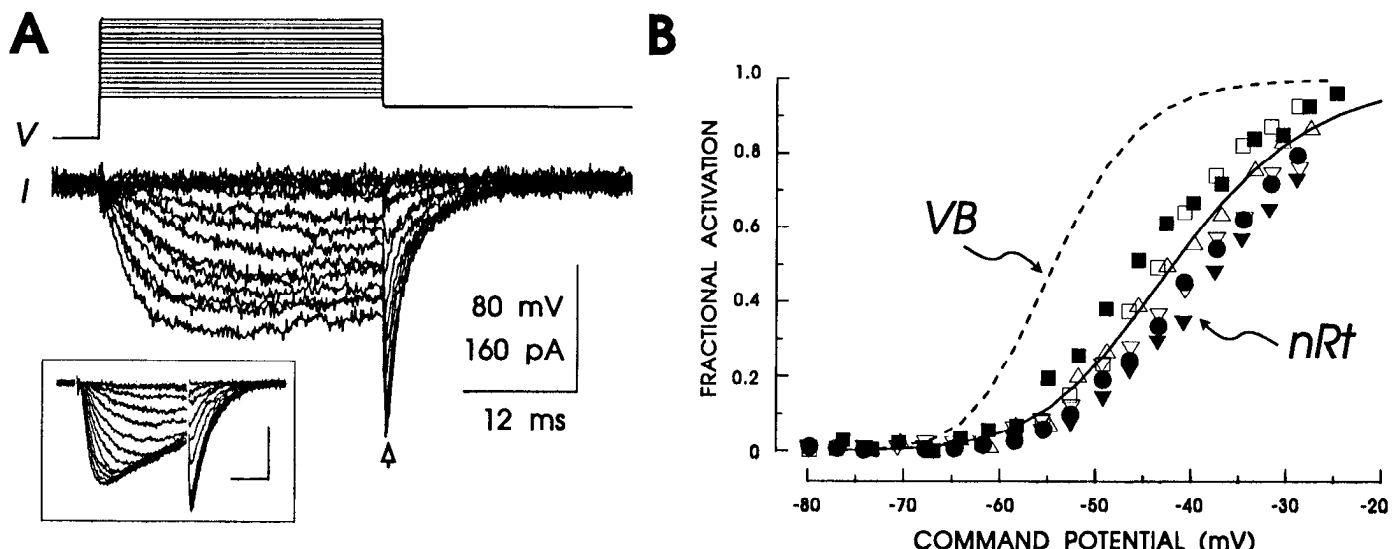


Figure 5. Activation curve for I_T in nRt cells. *A*, I_T was activated with 30 msec depolarizations from -100 mV to various potentials, and tail currents were obtained upon return to -80 mV. The inset depicts currents obtained with the same protocol in a VB neuron. *B*, Normalized tail current amplitude for five different nRt cells (Δ is from *A*, measured at the latency indicated by the arrow) versus command potential. The continuous curve is the best-fitted squared Boltzmann curve with $V_{1/2} = -49$ mV and $k = -6.5$ mV $^{-1}$, and the discontinuous curve is the average activation curve for VB neurons with $V_{1/2} = -59$ mV and $k = -5.2$ mV $^{-1}$.

Steady-state inactivation was investigated with standard protocols. The holding potential was set to -60 mV, and depolarizations to -30 mV were repeated at regular intervals (10 sec). A 1 sec prepulse at potentials in the range of -110 to -40 mV preceded each depolarization. I_{Ts} was largest with the most hyperpolarized prepotentials and became smaller as the prepotentials were made less negative (Fig. 4*A*). The rate of decay of I_{Ts} was not affected by the amplitude of the current, providing evidence that a single population of channels underlies the whole-cell current. Current amplitude, normalized to maximum, is plotted as the shaded circles in the h_∞ curve in Figure 4*B*. The solid line is the best-fitted Boltzmann function

$$\frac{I}{I_{\max}} = \left(\frac{1}{1 + \exp\left(\frac{(V - V_{1/2})}{k}\right)} \right)^N, \quad (1)$$

with $k = 5.3$ mV $^{-1}$, $V_{1/2} = -80$ mV, $I_{\max} = 164$ pA, and $N = 1$. Normalized data from five other nRt cells are also included in Figure 4*B*. The discontinuous line is the average Boltzmann curve for steady-state inactivation of I_T in VB cells, and is quite similar to the nRt data. Group data verified that $V_{1/2}$ is not different between the two cell types, but showed that the slope is slightly steeper for I_T than for I_{Ts} (Table 1). Thus, by this criterion, I_{Ts} is much more similar to I_T than to I_N .

Voltage-dependent activation of I_{Ts}

Since calcium currents are not characterized by a true reversal potential, it is not practical to obtain normalized activation curves by plotting conductance (current divided by driving force) versus voltage. An alternate approach is to step depolarize to command potentials in the activation range for I_{Ts} and, at a fixed latency near peak current, repolarize to a hyperpolarized potential outside the activation range, and then measure tail current amplitude. The currents thus obtained reflect the channels activated during the depolarization, and since the tail potential is fixed, currents can be normalized to maximum and plotted versus command potential to generate an activation curve. To study I_{Ts} in nRt cells, 30 msec depolarizing commands were applied and tail currents were obtained at -80 mV (Fig. 5*A*). The most depolarized commands produced nearly overlapping tail currents, indicating that activation was at or near saturation. With further depolarizations, tail currents were contaminated by I_L , so it was not possible to obtain maximal activation of I_{Ts} in isolation. In Figure 5*B*, upright triangles represent normalized tail current amplitude for the cell in Figure 5*A*, and the continuous line is the best-fitted squared Boltzmann curve (Eq. 1), with $k = -8.4$ mV $^{-1}$, $V_{1/2} = -49$ mV, and $N = 2$. The activation of I_{Ts} was nearly complete at -20 mV, which further differentiates it from I_N . Activation of I_T in VB cells, measured with the same protocol, occurred at significantly less depolarized levels (Fig. 5*A*, inset; *B*, discontinuous line; Table

Table 1. Steady-state inactivation and activation parameters for I_{Ts} versus I_T

	Activation (m_∞)		Inactivation (h_∞)	
	nRt	VB	nRt	VB
$V_{1/2}$ (mV)	-50 ± 2.3 (6)*	-59 ± 1.7 (30)	-78 ± 0.7 (20)	-81 ± 1.2 (25)
Slope (mV $^{-1}$)	-7.4 ± 1.1 (6)	-5.2 ± 0.5 (30)	5.0 ± 0.2 (20)*	4.4 ± 0.2 (20)

Currents were evoked using the protocols given in the methods. Values are results of best-fitted curves to equation 1 with $n = 2$ for activation and $n = 1$ for inactivation. Numbers of cells are given in parentheses.

* Two tailed t test, $p < 0.05$ compared to VB.

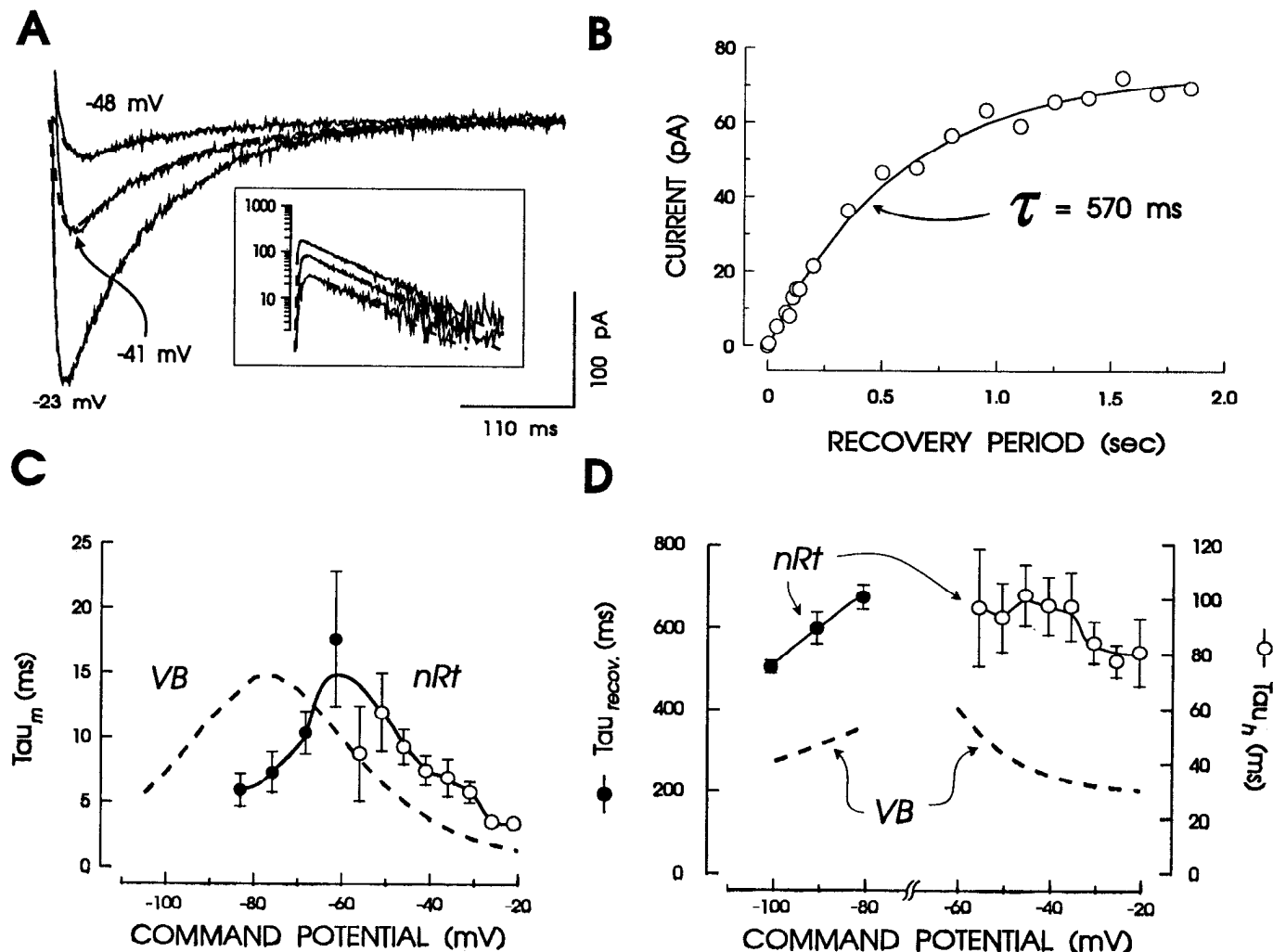


Figure 6. Voltage-dependent kinetics for I_T activation and inactivation in nRt neurons. *A*, Representative traces with overlaid m^2h Hodgkin-Huxley fitted curves. In the inset, semilog graphs are shown for both the current traces and the fitted curves. Fitting parameters at -48, -41, and -23 mV were 10, 6.6, and 3.7 msec for τ_m and 100, 97, and 89 msec for τ_h . *B*, Recovery from inactivation for I_T . The holding potential was set to -40 mV, and 50 mV hyperpolarizations of incrementing duration were applied. I_T peak amplitude was measured upon return to -40 mV. The recovery curve followed a monoexponential time course, best fitted with a time constant of 570 msec. *C*, Voltage dependence of τ_m . Open circles (\circ) are from the results of least-squares fitted curves as in *A* (5–11 cells at each point). Solid circles (\bullet ; $n = 4$) are from fitted exponential decay curves of tail currents (see Fig. 5) obtained at different potentials. τ_m was determined as $2 \times \tau_{tail}$. The discontinuous line is τ_m for I_T in VB cells. Error bars are SEM. *D*, Voltage dependence of τ_h . Solid circles (left axis; $n = 4$) are from recovery from inactivation as in *B*, while open circles (right axis; $n = 5$) are rates of inactivation from fitted current traces as in *A*. Note differences in vertical scale. Voltage dependence of τ_h for VB is indicated by the discontinuous line.

1). Because some inactivation occurs during the depolarizing command step, tail current amplitudes do not directly provide the activation curve, especially for I_T since it decays rapidly in comparison to the step duration. Even taking this into account, I_T activated with a lower threshold and was completely activated at less depolarized potentials when compared to I_{Ts} .

Voltage-dependent kinetics of I_{Ts}

As demonstrated in Figure 3, one of the major differences between I_T and I_{Ts} is the rate of inactivation. To examine further the voltage dependence of activation and inactivation rates for I_{Ts} , transient Ca^{2+} currents, isolated as in the methods of Figure 3*B*, were fitted with the following curve (based on Hodgkin and Huxley, 1952):

$$I_{\text{Ca}} = \left[1 - \exp\left(-\frac{t}{\tau_m}\right) \right]^2 \times \exp\left(-\frac{t}{\tau_h}\right) \times I_\infty, \quad (2)$$

where t is time, τ_h is the inactivation time constant, τ_m is the activation time constant, and I_∞ is an amplitude scaling factor. Evoked current decay curves, plotted on a semilog graph, were parallel (Fig. 6*A*, inset), indicating that the inactivation time constant, τ_h , was nearly independent of membrane potential in the range of -60 to -20 mV (open symbols, Fig. 6*D*). This contrasts sharply with the values for VB neurons (Fig. 6*D*, discontinuous line), which are highly voltage dependent, decreasing from 60 to 30 msec in the same voltage range. The time- and voltage-dependent process of recovery from inactivation (or deactivation), which controls the return of availability of channels subsequent to inactivation and is thus an important factor in determining the rate of repetitive LTS generation in TCs (Llinás and Jahnsen, 1982; Coulter et al., 1989a), was quite slow for I_{Ts} , with a time constant near 600 msec at -90 mV (Fig. 6*B,D*, solid symbols) compared to 350 msec for I_T in VB cells. Activation time constants (open circles, Fig. 6*C*) were

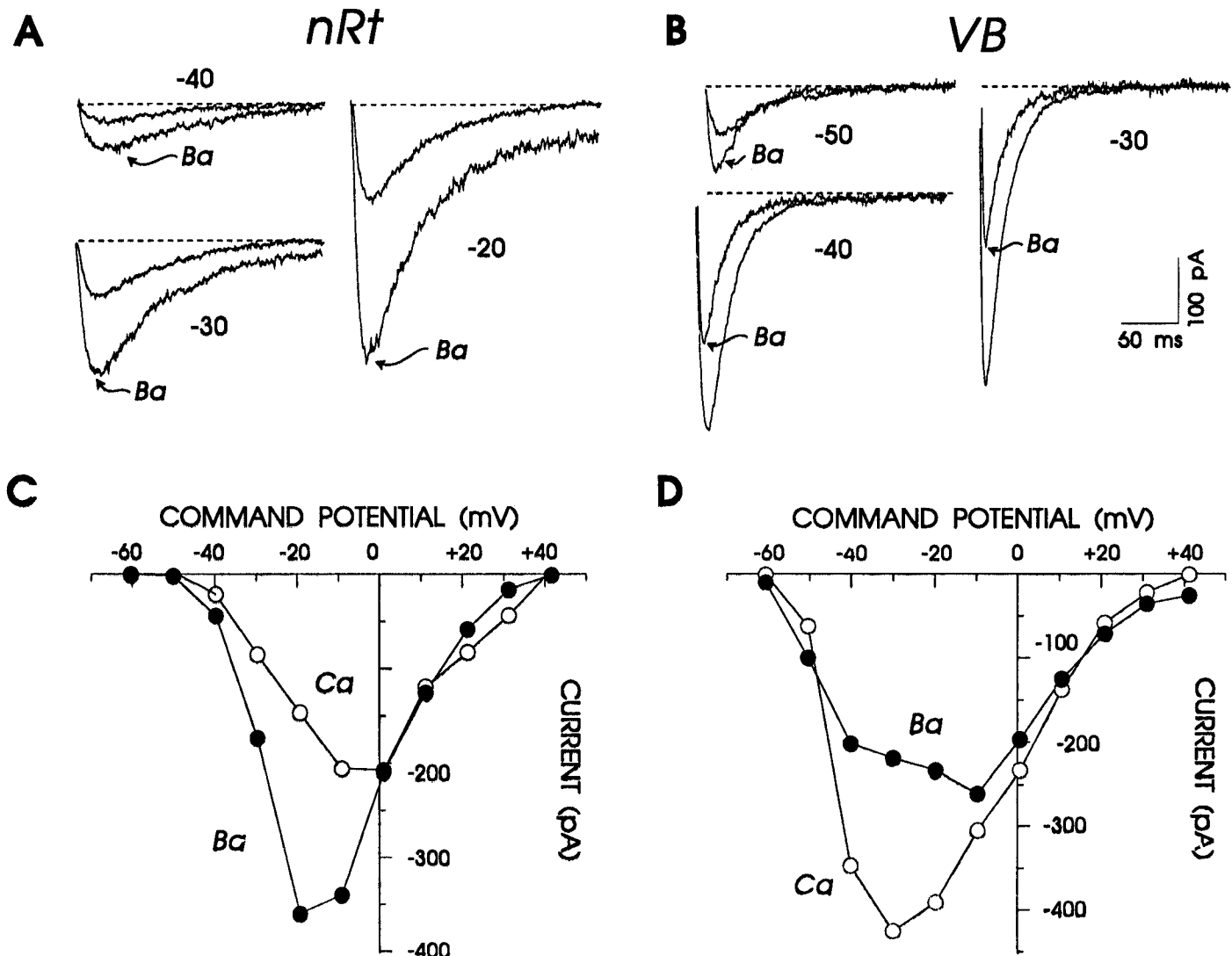


Figure 7. Barium as a charge carrier for I_T and I_{T_s} . *A*, Voltage-inactivated current in an nRt cell with 3 mM Ca^{2+} or 3 mM Ba^{2+} as the charge carrier. In these cells, the current was larger with Ba^{2+} than Ca^{2+} . The currents traces were obtained as in Figure 3*B*. *B*, In VB neurons, with depolarizations positive to -50 mV, I_T was smaller with Ba^{2+} than with Ca^{2+} . *C* and *D*, I - V curves for the voltage-inactivated current in nRt and VB.

determined from current traces fitted to Equation 2 as in Figure 6*A*, and deactivation rate was obtained by fitting a single exponential decay curve to the tail currents. Since I_{T_s} inactivation is relatively slow (Fig. 6*D*), the rapid tail currents at hyperpolarized potentials represent reversal of the activation process (deactivation) rather than inactivation, and assuming m^2h kinetics, the time constant of deactivation (Fig. 6*C*, solid circles) was estimated as two times the tail current time constant (Kay and Wong, 1987). The values of τ_m for VB neurons are given as the discontinuous curve in Figure 6*C*. In both cell types activation kinetics are characterized by a bell-shaped voltage dependence, with time constant values ranging from 2 to 15 msec. However, the peak of the curve is shifted by approximately +20 mV in nRt cells, so that in the LTS generation range of -60 to -40 mV, activation is approximately twice as fast in VB compared to nRt.

Barium as a charge carrier for I_{T_s}

For many L- or high-voltage-activated (HVA) type Ca^{2+} channels, Ba^{2+} is a more permeant charge carrier than Ca^{2+} , so

currents are significantly larger when Ba^{2+} is used (Fedulova et al., 1985; Carbone and Lux, 1987*a,b*; Fox et al., 1987). However, for T-currents, peak amplitude tends to be either comparable or slightly smaller when Ca^{2+} is replaced with Ba^{2+} (Fedulova et al., 1985; Carbone and Lux, 1987*a,b*; Fox et al., 1987). In nRt cells, substitution of 3 mM $[\text{Ba}^{2+}]_o$ for $[\text{Ca}^{2+}]_o$ resulted in significantly larger I_{T_s} (Fig. 7*A*, Table 2). At all potentials between -40 and 0 mV, I_{Ba} was greater than I_{Ca} , but there was little change in the kinetics of the current. In contrast, the transient current in VB cells was reduced by Ba^{2+} at potentials between -40 and 0 mV, and was slightly enhanced at -50 mV (Fig. 7*B*). In addition, the rate of I_T decay in VB cells was increased in Ba^{2+} (Fig. 7*B*). Since I_T decay rate is voltage dependent (i.e., becomes faster with depolarization), these findings are consistent with a presumed reduction in the transmembrane electric field resulting from less effective screening charge (Frankenhaeuser and Hodgkin, 1957) produced by Ba^{2+} compared to Ca^{2+} . The screening charge difference would result in reduction in current amplitude by reducing the steady-state availability of I_T channels (see Fig. 6), and in fact the steady-

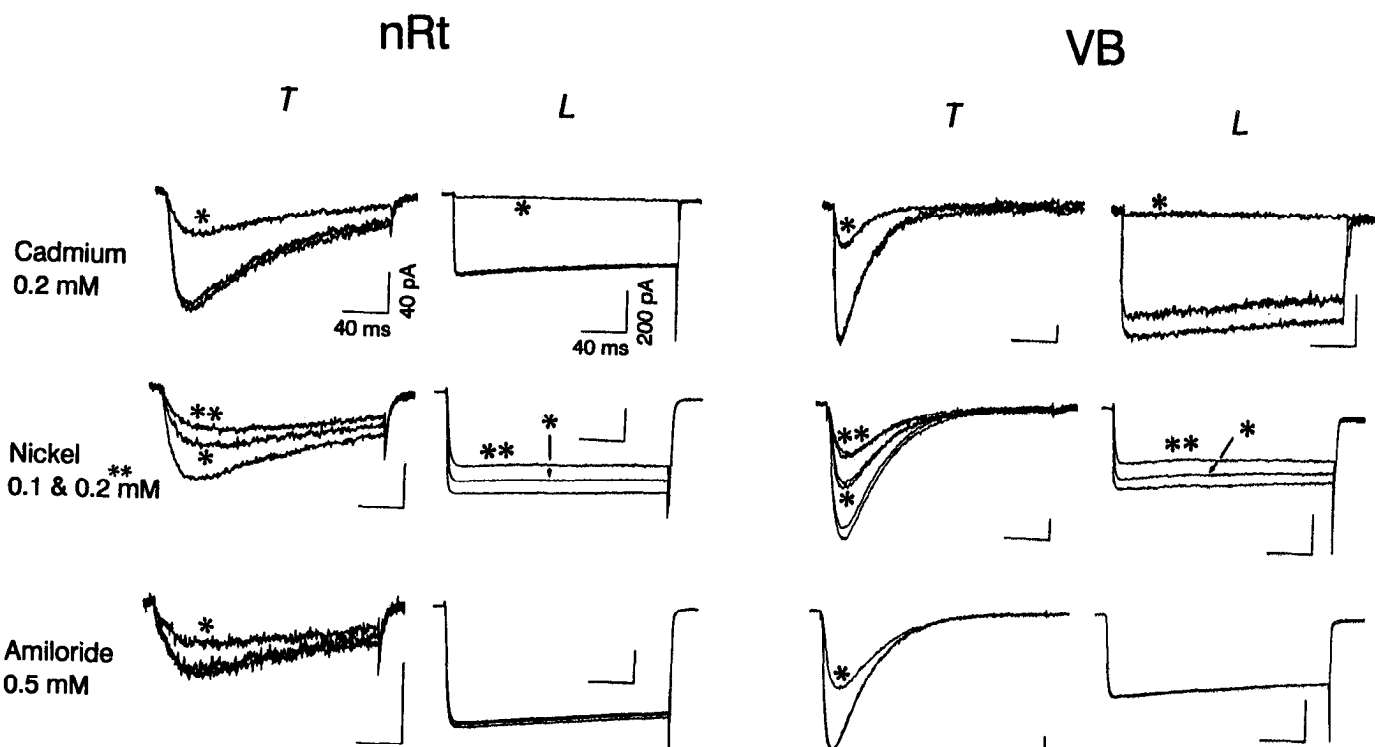


Figure 8. Pharmacology of I_{Ca} in thalamic neurons. T-currents were evoked by depolarizing to -40 from -100 mV, while L-currents were evoked by depolarizing from -50 to $+10$ mV. An asterisk (*) marks currents obtained while drugs were applied. Where two control traces are present (Cd^{2+} and amiloride), one was obtained after drug application. Calibration for T-current in top left panel applies for all T-currents, while for L-currents 200 pA is the vertical calibration.

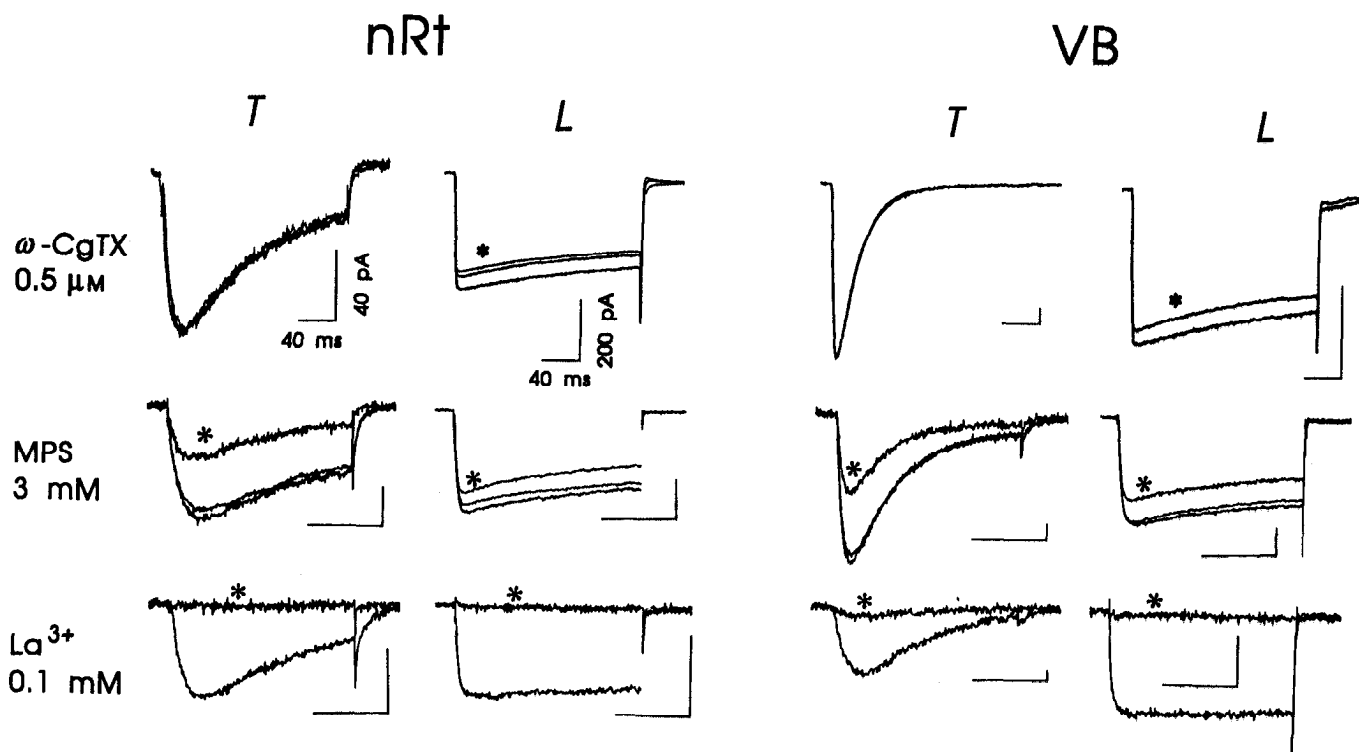


Figure 9. Continued I_{Ca} pharmacology with ω -CgTx, MPS, and lanthanum. The protocols and calibration bars are the same as in Figure 8.

Table 2. Ca^{2+} current pharmacology in nRt versus VB neurons

	T-current		L-current	
	nRt	VB	nRt	VB
$\text{Cd}^{2+}, 0.2 \text{ mM}$	39 ± 2.0 (3)	35 ± 1.5 (5)	3.0 ± 0.2 (3)†††	3.6 ± 1.7 (5)†††
$\text{Ni}^{2+}, 0.1 \text{ mM}$	66 ± 6.4 (2)	57 ± 3.3 (4)	82 ± 5.7 (2)	84 ± 2.5 (4)†††
$\text{Ni}^{2+}, 0.2 \text{ mM}$	46 ± 6.4 (2)*	34 ± 1.9 (4)	66 ± 6.4 (2)	64 ± 4.2 (4)†††
$\text{La}^{3+}, 0.1 \text{ mM}$	3.3 ± 0.8 (2)	1.0 ± 1.2 (3)	4.5 ± 2.1 (2)	3.3 ± 0.8 (3)
Amiloride, 0.5 mM	59 ± 13 (2)	62 ± 2.6 (3)	96 ± 2.8 (2)	99 ± 1.1 (3)†††
$\omega\text{-CgTx}, 0.5 \mu\text{M}$	102 ± 4.8 (3)	98 ± 2.8 (2)	82 ± 12 (3)	82 ± 2.0 (2)†
$\text{Ba}^{2+}, 3 \text{ mM}$	150 ± 14 (7)***	66 ± 6.4 (5)	100 ± 11 (7)†	106 ± 9.1 (3)††
MPS, 3 mM	47 ± 0.7 (2)	48 ± 1.2 (4)	71 ± 1.4 (2)††	76 ± 3.2 (4)†††
Bay E9736, 1 μM	99 ± 1.4 (4)	100 ± 0 (2)	88 ± 3.4 (4)†	85 ± 7.1 (2)
Bay K8644, 1 μM	114 ± 5.2 (5)	102 ± 2.8 (2)	139 ± 12 (5)	164 ± 24 (2)

Currents were evoked using the protocols given in the methods. Values are peak current amplitude expressed as a percentage of control, and represent average ± SEM. Numbers of cells are given in parentheses. Two tailed *t*-test: **p* < 0.05; ****p* < 0.001, compared to VB; †*p* < 0.05, ††*p* < 0.01, †††*p* < 0.001 compared to T-current within the same cell type.

state inactivation curve was shifted by $-6.6 \pm 0.9 \text{ mV}$ ($n = 7$) in the presence of Ba^{2+} . However, maximum I_t amplitude was still smaller with Ba^{2+} compared to Ca^{2+} , even when all command potentials were hyperpolarized to compensate for this shift (not shown; $n = 3$). Therefore, I_{ts} has permeation properties that are more similar to I_L than to I_t . These differences in whole-cell current may be due to various single-channel mechanisms including higher channel conductance or altered kinetic parameters such as higher open probability or open duration.

Pharmacology of I_t in nRt versus VB cells

Apart from the kinetic differences discussed above, I_{ts} in nRt cells is similar to I_t in relay neurons since both are transient, low-voltage-activated currents, but I_{ts} also shows some similarity to the “N”-current, since I_N activates at a higher threshold than I_t , but shows slow inactivation (Fox et al., 1987). However, a number of pharmacological differences were present between I_t and the slower currents (I_N and I_L ; Fox et al., 1987) activated with stronger depolarizations, which allows a clear differentiation between these separate conductances. For example, I_N and I_L are sensitive to blockade by Cd^{2+} (Fox et al., 1987), but both I_t and I_{ts} were relatively spared by concentrations of Cd^{2+} that eliminated I_L in thalamic neurons (Fig. 8, Table 2). On the other hand, Ni^{2+} (100–200 μM), which is a somewhat selective blocker of I_t , produced similar reductions in I_{ts} , yet had smaller effects on I_L (Fig. 8). Therefore, I_{ts} is more similar to I_t than to I_N in terms of its sensitivity to divalent blockers. Another agent that can be used to differentiate between various Ca^{2+} currents is amiloride (Tang et al., 1988). At a concentration of 0.5 mM, it reversibly blocked both I_t and I_{ts} , but had little effect on I_L in either cell type (Fig. 8).

One of the hallmarks of N-current is sensitivity to $\omega\text{-CgTx}$. This cone snail peptide toxin (Olivera et al., 1985) produces a potent and irreversible block of N-type calcium current, and may inhibit I_L as well (McCleskey et al., 1987). To differentiate further between I_t and I_N , the applications of 0.5 μM $\omega\text{-CgTx}$ were tested and found to result in a rapid, partial, and irreversible block of I_L in both nRt and VB cells (Fig. 9), while I_t and I_{ts} were unaffected in both cell types. Succinimide anticonvulsants produce a relatively selective blockade of I_t in VB cells (Coulter et al., 1989b, 1990), and we therefore tested the effects of one such agent on Ca^{2+} currents in nRt. Methylphenylsuccinimide (MPS; 3 mM; Fig. 9) reduced both I_t and I_{ts} by approximately 50% (Table 2), while I_L was reduced by only 25%. Dihydropyridines, which are somewhat selective in their effects on I_L (Fox et al., 1987; Takahashi and Akaike, 1991) were relatively ineffective in depressing the transient currents in thalamic cells. Nimodipine (Bay E9736; nominally 1 μM) produced small reversible reductions in L-current in both cell types (Table 2), while sparing I_t . The small reductions (10–15%) in “L”-currents by either dihydropyridines or $\omega\text{-CgTx}$ are similar to the incomplete blockade seen in cerebellar Purkinje cells and hippocampal CA1 neurons (Regan et al., 1991). The calcium channel agonist Bay K8644 enhanced I_L but not I_t in VB cells (Table 2). However, its effects were slightly less selective in nRt cells, where, in addition to the augmentation of I_L , Bay K8644 produced a slight enhancement of I_{ts} (114% of control; Table 2).

In isolated nRt cells, I_{ts} was quite stable, like I_t in VB cells, and unlike I_L , which washes out during prolonged recording. With the inclusion of the ATP regeneration system (see Materials and Methods) in the pipette solution, I_L became less labile. However, the amplitude of I_L did typically increase to a maximal level during the first 5–10 min of recording and then gradually wash out for the remainder of the experiment, while both I_{ts} and I_t maintained a fairly constant peak amplitude throughout the recording. A further similarity between the two forms of I_t was that both were apparently insensitive to Ca^{2+} -dependent inactivation. While I_t is relatively insensitive to intracellular Ca^{2+} concentration (Carbone and Lux, 1987a), HVA currents are reduced by either elevated $[\text{Ca}^{2+}]$ (Carbone and Lux, 1987a) or reduced Ca^{2+} -buffering capacity (Meyers and Barker, 1989). Both I_t and I_{ts} persisted during recordings made with $[\text{Ca}^{2+}]$ elevated to 0.5 μM , while I_L was either greatly reduced or absent ($n = 6$). To summarize, the pharmacology and metabolic properties of I_{ts} are very similar to I_t and quite distinct from those of I_N and I_L .

Discussion

Identity of I_{ts}

Because I_{ts} was larger in Ba^{2+} than Ca^{2+} and inactivated slowly and in a voltage-independent manner, we considered that it might be the same as the N-current seen in chick dorsal root ganglion (DRG) cells (Fox et al., 1987). However, nearly every

test that we applied demonstrated that I_{Ts} was a distinct current. Whereas I_N is blocked by ω -CgTx and Cd^{2+} (Fox et al., 1987), I_{Ts} was much less affected. The gating of I_{Ts} and I_N is also different in that the voltage range of activation of I_N is broader and more depolarized than for I_{Ts} , and steady-state inactivation of I_{Ts} occurs at more negative potentials. Both I_L and I_N appear to depend on intracellular factors that "wash out" during whole-cell recordings made without ATP in the patch electrode solution (Fedulova et al., 1985; Forscher and Oxford, 1985; Meyers and Barker, 1989; Ryu and Randic, 1990), and HVA currents are decreased when intracellular Ca^{2+} buffering is reduced (Carbone and Lux, 1987a,b; Meyers and Barker, 1989). By contrast, I_{Ts} was quite stable (like I_T) during whole-cell recordings even with elevated $[Ca^{2+}]_i$. We conclude that I_{Ts} is not the same as I_N in the traditional sense. Furthermore, I_{Ts} is different from two other voltage-gated Ca^{2+} currents, I_L (Carbone and Lux, 1987a; Fox et al., 1987) and I_P (Llinás et al., 1989), in that these currents are activated at higher thresholds and are only very slowly inactivating.

On the other hand, there were similarities between I_T in relay neurons and I_{Ts} in neurons of the nRt. Both currents were selectively blocked by Ni^{2+} , amiloride, and MPS and were resistant to ω -CgTx and dihydropyridines. In addition, steady-state inactivation properties were similar. However, I_{Ts} was not identical to I_T in that there were differences in voltage-dependent activation, voltage-dependent inactivation rate, and $Ba^{2+}:Ca^{2+}$ permeability ratio. The voltage *insensitivity* of inactivation of I_{Ts} stands in striking contrast to the voltage *dependency* of inactivation of macroscopic T-currents in cells from a diverse group of other preparations (rat and chick DRG: Carbone and Lux, 1987a,b; Fox et al., 1987; rat somatosensory thalamus: Coulter et al., 1989a; rat cerebellum: Kaneda et al., 1990; rat hippocampus: Takahashi et al., 1991; guinea pig olfactory cortex: Constanti et al., 1985; rat sensorimotor cortex: Sayer et al., 1990; neuroblastoma cells from mouse and man: Narahashi et al., 1987; Carbone et al., 1990; fibroblasts: Chen and Hess, 1990; pituitary gonadotrophs: Mason and Sikdar, 1989; canine cardiac Purkinje cells: Hirano et al., 1989; guinea pig ventricular cells: Droogmans and Nilius, 1989). Furthermore, in experiments where permeation properties for I_T have been analyzed, Ba is either equally or less effective as a charge carrier than Ca (Bossu et al., 1985; Fedulova et al., 1985; Carbone and Lux, 1987a,b; Fox et al., 1987; Tsien et al., 1987; Droogmans and Nilius, 1989; Hirano et al., 1989; Carbone et al., 1990; Takahashi et al., 1991; but see Yoshii et al., 1988). These differences justify designation of the transient Ca^{2+} current in nRt as a new subtype of T-current that we have termed I_{Ts} .

The elucidation of the molecular mechanisms underlying the macroscopic differences in I_{Ts} and I_T will require single-channel recordings. The inactivation rate of single T-channels is voltage independent (Carbone and Lux, 1987b; Droogmans and Nilius, 1989; Chen and Hess, 1990), and the voltage-dependent decay of ensemble macroscopic current is actually the result of a voltage-dependent channel opening step and a voltage-dependent single-channel burst duration. The lack of voltage-dependent macroscopic inactivation suggests that there are fundamental differences in the gating properties of I_{Ts} compared to I_T .

Functional implications

The unique properties of I_{Ts} have important consequences for thalamic function. Because the rate of I_{Ts} inactivation is slow ($\tau_h \approx 90$ msec) and *voltage independent*, the resulting LTS, which

serves as the generator potential for bursts of Na^+ spikes, is less self-limiting than in relay neurons, where the depolarization induced by the LTS speeds inactivation of T-current. Thus, spike bursts are relatively prolonged in nRt cells, and as a consequence large IPSPs with prominent K^+ -mediated GABA_A components will be produced in TCs. Intracellular recordings in TCs have shown that deinactivation of T-channels requires prolonged hyperpolarization (~100 ms; Jähnichen and Llinás, 1984; Coulter et al., 1989a). Therefore, these large IPSPs, especially the K^+ -mediated components, would facilitate rebound LTSs. Because of the reciprocal connections with cortex and nRt, bursts in excitatory efferents from TCs to nRt and cortex that result from such LTS generation can promote a reverberatory rhythm. Therefore, burst firing in nRt, mediated by I_{Ts} , may be a critical factor in initiating intrathalamic and thalamocortical oscillations. Succinimide anticonvulsants, which block I_T in VB neurons (Coulter et al., 1989b, 1990), are also effective in reducing I_{Ts} in nRt. These two cellular actions may contribute to the clinical efficacy of these agents in petit mal epilepsy. Since burst firing in nRt is thought to be critical for thalamocortical synchronization, reduction in burst firing through blockade of I_{Ts} would be expected to have antiepileptic effects. The results of *in vivo* experiments support of this hypothesis. Ethosuximide, a compound in the succinimide class, reduces burst firing frequency and increases tonic firing in nRt at the cellular level, while at the same time reducing both intrathalamic and thalamocortical synchronization at the circuit level (Pellegrini et al., 1989).

The smaller amplitude of I_{Ts} and higher voltage for activation might reduce the likelihood of obtaining an LTS in nRt cells compared to TCs; however, input resistance tends to be higher in nRt neurons (McCormick and Prince, 1986) than in TCs, and this may counter both effects. The rate of deinactivation of I_{Ts} is relatively slow (time constant ~600 msec at -90 mV, 23°C; Fig. 6D). If we assume a temperature coefficient of 3 (Coulter et al., 1989a), the resultant time constant would be approximately 135 msec at 37°C. This would be sufficiently rapid to allow significant (52–65%) recovery of I_{Ts} within the intraspindle frequency (7–10 Hz), and thus maintain a prolonged rhythm.

Since the rate of activation of I_{Ts} is somewhat slower than that for I_T (Fig. 6C), the current will peak later in nRt cells than in TCs. This may partially explain the acceleration in spike frequency within the early portions of nRt bursts seen *in vivo* (Domich et al., 1986; Pellegrini et al., 1989), since maximal frequency should occur near the time of peak I_{Ts} activation. The slowing of spike frequency observed late in the burst *in vivo* (Domich et al., 1986) is probably due to the slow inactivation of I_{Ts} . This same burst pattern (early acceleration followed by late deceleration) can also be observed *in vitro*, although this is not clearly shown in the compressed time base of Figure 1. Interestingly, since I_{Ts} activates at more depolarized levels than I_T (Fig. 5B), in the absence of confounding differences in other ionic conductances, the threshold for LTSs should then be relatively depolarized in nRt.

One prediction from these findings (see Fig. 7) is that Ba^{2+} substitution for Ca^{2+} should produce conditions whereby burst firing is selectively promoted in nRt compared to relay nuclei within thalamic slices because I_{Ts} would be enhanced while I_T is inhibited. This effect would be somewhat complicated by the effects of Ba^{2+} on Ca^{2+} channel inactivation (Fedulova et al., 1985; Carbone and Lux, 1987a; Meyers and Barker, 1989) and

K^+ channel blockade (Krnjevic et al., 1971). However, given the marked enhancement of I_{Ts} by Ba^{2+} (~200% increase; see Fig. 7), cell-specific differences should still be apparent.

The results of this comparison of T-current in nRt and VB provide further evidence supporting the hypothesis that neurons with different functional roles within a circuit are likely to have different biophysical properties, determined at least in part by quantitative and/or qualitative differences in voltage-dependent ion channels. For example, many interneurons in the hippocampus and neocortex are capable of firing at higher frequencies than pyramidal cells (Schwartzkroin and Mathers, 1978; McCormick et al., 1985), an observation that can be explained in part by both the lack of A-current (Hamill et al., 1991) and Ca^{2+} -dependent afterpotentials (McCormick et al., 1985) in interneurons. Deciphering the functional implications of the large numbers of diverse channel subtypes described in recent studies (e.g., K^+ : Rudy, 1988; Reinhart et al., 1989; Stühmer et al., 1989; Na^+ : Noda et al., 1986; Auld et al., 1988; Trimmer and Agnew, 1989; Ca^{2+} : Miller, 1987; Hui et al., 1991; Snutch et al., 1991) may seem an overwhelming task. However, data such as those presented here suggest that, when other variables such as the neurons' receptor subtypes, transmitter phenotype, and position in the circuit are taken into account, even subtle differences between channel species can be shown to have a clear functional role within the rich fabric of the brain.

References

- Auld VJ, Goldin AL, Kraft DS, Marshall J, Dunn JM, Catterall WA, Lester HA, Davidson N, Dunn RJ (1988) A rat brain Na^+ channel α subunit with novel gating properties. *Neuron* 1:449–461.
- Avanzini G, deCurtis M, Panzica F, Spreafico R (1989) Intrinsic properties of nucleus reticularis thalami neurones of the rat studied *in vitro*. *J Physiol (Lond)* 416:111–122.
- Blanton MG, Lo Turco JJ, Kriegstein AR (1989) Whole cell recording from neurons in slices of reptilian and mammalian cerebral cortex. *J Neurosci Methods* 30:203–210.
- Bossu JL, Feltz A, Thomann JM (1985) Depolarization elicits two distinct calcium currents in vertebrate sensory neurons. *Pfluegers Arch* 403:360–368.
- Carbone E, Lux HD (1987a) Kinetics and selectivity of a low-voltage-activated calcium current in chick and rat sensory neurones. *J Physiol (Lond)* 386:547–570.
- Carbone E, Lux HD (1987b) Single low-voltage-activated calcium channels in chick and rat sensory neurones. *J Physiol (Lond)* 386:571–601.
- Carbone E, Sher E, Clementi F (1990) Ca Currents in human neuroblastoma IMR32 cells: kinetics, permeability and pharmacology. *Pfluegers Arch* 416:170–179.
- Chen C, Hess P (1990) Mechanism of gating of T-type calcium channels. *J Gen Physiol* 96:603–630.
- Constanti A, Galvan M, Franz P, Sim JA (1985) Calcium-dependent inward currents in voltage-clamped guinea-pig olfactory cortex neurones. *Pfluegers Arch* 404:259–265.
- Coulter DA, Huguenard JR, Prince DA (1989a) Calcium currents in rat thalamocortical relay neurones: kinetic properties of the transient, low-threshold current. *J Physiol (Lond)* 414:587–604.
- Coulter DA, Huguenard JR, Prince DA (1989b) Characterization of ethosuximide reduction of low-threshold calcium current in thalamic neurons. *Ann Neurol* 25:582–593.
- Coulter DA, Huguenard JR, Prince DA (1990) Differential effects of petit mal anticonvulsants and convulsants on thalamic neurones: calcium current reduction. *Br J Pharmacol* 100:800–806.
- Crunelli V, Lightowler S, Pollard CE (1989) A T-type Ca^{2+} current underlies low-threshold Ca^{2+} potentials in cells of the cat and rat lateral geniculate nucleus. *J Physiol (Lond)* 413:543–561.
- Deschénes M, Roy JP, Steriade M (1982) Thalamic bursting mechanism: a slow inward current revealed by membrane hyperpolarization. *Brain Res* 239:289–293.
- Domich L, Oakson G, Steriade M (1986) Thalamic burst patterns in the naturally sleeping cat: a comparison between cortically projecting and reticularis neurones. *J Physiol (Lond)* 379:429–449.
- Droogmans G, Nilius B (1989) Kinetic properties of the cardiac T-type calcium channel in the guinea-pig. *J Physiol (Lond)* 419:627–650.
- Dutar P, Nicoll RA (1988) A physiological role for $GABA_B$ receptors in the central nervous system. *Nature* 332:156–158.
- Fedulova SA, Kostyuk PG, Veselovsky NS (1985) Two types of calcium channels in the somatic membrane of new-born rat dorsal root ganglion neurones. *J Physiol (Lond)* 359:431–446.
- Forscher P, Oxford GS (1985) Modulation of calcium channels by norepinephrine in internally dialyzed avian sensory neurons. *J Gen Physiol* 85:743–763.
- Fox AP, Nowycky MC, Tsien RW (1987) Kinetic and pharmacological properties distinguishing three types of calcium currents in chick sensory neurons. *J Physiol (Lond)* 394:149–172.
- Frankenhaeuser B, Hodgkin AL (1957) The action of calcium on the electrical properties of squid axons. *J Physiol (Lond)* 137:218–244.
- Hamill OP, Marty A, Neher E, Sakmann B, Sigworth FJ (1981) Improved patch-clamp techniques for high-resolution current recording from cells and cell-free membrane patches. *Pfluegers Arch* 391:85–100.
- Hamill OP, Huguenard JR, Prince DA (1991) Patch clamp studies of voltage gated currents in identified neurons of the rat cerebral cortex. *Cereb Cortex* 1:48–61.
- Harris RM, Hendrickson AE (1987) Local circuit neurons in the rat ventrobasal thalamus—a GABA immunocytochemical study. *Neuroscience* 21:229–236.
- Hernández-Cruz A, Pape H-C (1989) Identification of two calcium currents in acutely dissociated neurons from the rat lateral geniculate nucleus. *J Neurophysiol* 61:1270–1283.
- Hirano Y, Fozzard HA, January CT (1989) Characteristics of L- and T-type Ca^{2+} currents in canine cardiac Purkinje cells. *Am J Physiol* 256:H1428–H1492.
- Hodgkin AL, Huxley AF (1952) A quantitative description of membrane current and its application to conduction and excitation in nerve. *J Physiol (Lond)* 117:500–544.
- Huguenard JR, Prince DA (1991) An unconventional transient Ca current in GABAergic neurons of rat thalamic reticular nucleus. *Soc Neurosci Abstr* 17:342.
- Hui A, Ellinor PT, Krizanova O, Wang J-J, Diebold RJ, Schwartz A (1991) Molecular cloning of multiple subtypes of a novel rat brain isoform of the α subunit of the voltage-dependent calcium channel. *Neuron* 7:35–44.
- Jahnsen H, Llinás R (1984) Electrophysiological properties of guinea-pig thalamic neurones: an *in vitro* study. *J Physiol (Lond)* 349:205–226.
- Jones EG (1985) The thalamus. New York: Plenum.
- Kaneda M, Wakamori M, Ito C, Akaike N (1990) Low-threshold calcium current in isolated Purkinje cell bodies of rat cerebellum. *J Neurophysiol* 63:1046–1051.
- Kay AR, Wong RKS (1986) Isolation of neurons suitable for patch-clamping from adult mammalian central nervous systems. *J Neurosci Methods* 16:227–238.
- Kay AR, Wong RKS (1987) Calcium current activation kinetics in isolated pyramidal neurones of the CA1 region of the mature guinea-pig. *J Physiol (Lond)* 392:603–616.
- Krnjevic K, Pumain R, Renaud L (1971) Effects of Ba^{2+} and tetraethylammonium on cortical neurones. *J Physiol (Lond)* 215:223–245.
- Llinás RR, Geijo-Barrientos E (1988) *In vitro* studies of mammalian thalamic and reticularis thalami neurons. In: Cellular thalamic mechanisms (Bentivoglio M, Spreafico R, eds), pp 23–33. Amsterdam: Excerpta Medica.
- Llinás R, Jahnsen H (1982) Electrophysiology of mammalian thalamic neurones *in vitro*. *Nature* 297:406–408.
- Llinás R, Sugimori M, Lin J-W, Cherksey B (1989) Blocking and isolation of a calcium channel from neurons in mammals and cephalocephalopods utilizing a toxin fraction (FTX) from funnel-web spider poison. *Proc Natl Acad Sci USA* 86:1689–1693.
- Mason WT, Sikdar SK (1989) Characteristics of voltage-gated Ca^{2+} currents in ovine gonadotrophs. *J Physiol (Lond)* 415:367–391.
- McCleskey EW, Fox AP, Feldman DH, Cruz LJ, Olivera BM, Tsien RW, Yoshikami D (1987) Omega-conotoxin: direct and persistent blockade of specific types of calcium channels in neurons but not muscle. *Proc Natl Acad Sci USA* 84:4327–4331.

- McCormick DA, Prince DA (1986) Acetylcholine induces burst firing in thalamic reticular neurones by activating a potassium conductance. *Nature* 319:402–405.
- McCormick DA, Connors BW, Lighthall JW, Prince DA (1985) Comparative electrophysiology of pyramidal and sparsely spiny stellate neurons of the neocortex. *J Neurophysiol* 54:782–805.
- Meyers DE, Barker JL (1989) Whole-cell patch-clamp analysis of voltage-dependent calcium conductances in cultured embryonic rat hippocampal neurons. *J Neurophysiol* 61:467–477.
- Miller RJ (1987) Multiple calcium channels and neuronal function. *Science* 235:46–52.
- Morison RS, Bassett DL (1945) Electrical activity of the thalamus and basal ganglia in decorticate cats. *J Neurophysiol* 8:309–314.
- Mulle C, Steriade M, Deschénes M (1985) Absence of spindle oscillation in the cat anterior thalamic nuclei. *Brain Res* 334:2169–2171.
- Mulle C, Madariaga A, Deschénes M (1986) Morphology and electrophysiological properties of reticularis thalami neurons in cat: *in vivo* study of a thalamic pacemaker. *J Neurosci* 6:134–145.
- Narashashi T, Tsunoo A, Ace M (1987) Characterization of two types of calcium channels in mouse neuroblastoma cells. *J Physiol (Lond)* 383:231–249.
- Noda M, Ikeda T, Kayano T, Suzuki H, Takeshima H, Kurasaki M, Takahashi H, Numa S (1986) Existence of distinct sodium channel messenger RNAs in rat brain. *Nature* 320:188–192.
- Olivera BM, Gray WR, Zeikus R, McIntosh JM, Varga J, Rivier J, de Santos V, Cruz LJ (1985) Peptide neurotoxins from fish-hunting cone snails. *Science* 230:1338–1343.
- Otis TS, Staley KJ, Mody I (1991) Inhibitory activity in mammalian brain slices generated by spontaneous release. *Brain Res* 545:142–150.
- Pellegrini A, Dossi RC, Dal Pos F, Ermani M, Zanotto L, Testa G (1989) Ethosuximide alters intrathalamic and thalamocortical synchronizing mechanisms: a possible explanation of its antiabsence effect. *Brain Res* 497:344–360.
- Regan LJ, Sah DWY, Bean BP (1991) Ca^{2+} channels in rat central and peripheral neurons: high-threshold current resistant to dihydropyridines and ω -conotoxin. *Neuron* 6:69–280.
- Reinhart PH, Chung S, Levitan IB (1989) A family of calcium-dependent potassium channels from rat brain. *Neuron* 2:1031–1041.
- Ribary U, Ioannides AA, Singh KD, Hasson R, Bolton JPR, Lado F, Mogilner A, Llinás R (1991) Magnetic field tomography of coherent thalamocortical 40-Hz oscillations in humans. *Proc Natl Acad Sci USA* 88:11037–11041.
- Rudy B (1988) Diversity and ubiquity of K channels. *Neuroscience* 25:729–749.
- Ryu PD, Randic M (1990) Low- and high-voltage-activated calcium currents in rat spinal dorsal horn neurons. *J Neurophysiol* 63:273–285.
- Sayer RJ, Schwindt PC, Crill WE (1990) High- and low-threshold calcium currents in neurons acutely isolated from rat sensorimotor cortex. *Neurosci Lett* 120:175–178.
- Schwartzkroin PA, Mathers LH (1978) Physiological and morphological identification of a nonpyramidal hippocampal cell type. *Brain Res* 157:1–10.
- Shosaku A, Kayama Y, Sumitomo I, Sugitani M, Iwama K (1989) Analysis of recurrent inhibitory circuit in rat thalamus: neurophysiology of the thalamic reticular nucleus. *Prog Neurobiol* 32:77–102.
- Snutch TP, Tomlinson WJ, Leonard JP, Gilbert M (1991) Distinct calcium channels are generated by alternative splicing and are differentially expressed in the mammalian CNS. *Neuron* 7:45–57.
- Spreafico R, de Curtis M, Frassoni C, Avanzini G (1988) Electrophysiological characteristics of morphologically identified reticular thalamic neurons from rat slices. *Neuroscience* 27:629–638.
- Steriade M, Llinás RR (1988) The functional states of the thalamus and the associated neuronal interplay. *Physiol Rev* 68:649–742.
- Steriade M, Deschénes M, Domich L, Mulle C (1985) Abolition of spindle oscillations in thalamic neurons disconnected from nucleus reticularis thalami. *J Neurophysiol* 54:1473–1497.
- Steriade M, Domich L, Oakson G (1986) Reticularis thalami neurons revisited: activity changes during shifts in states of vigilance. *J Neurosci* 6:68–81.
- Steriade M, Domich L, Oakson G, Deschénes M (1987) The deafferented reticular thalamic nucleus generates spindle rhythmicity. *J Neurophysiol* 57:260–273.
- Stühmer W, Ruppertsberg JP, Schröter KH, Sakmann B, Stocker M, Giese KP, Perschke A, Baumann A, Pongs O (1989) Molecular basis of functional diversity of voltage-gated potassium channels in mammalian brain. *EMBO J* 8:3235–3244.
- Suzuki S, Rogawski MA (1989) T-type calcium channels mediate the transition between tonic and phasic firing in thalamic neurons. *Proc Natl Acad Sci USA* 86:7228–7232.
- Takahashi K, Akaike N (1991) Calcium antagonist effects on low-threshold (T-type) calcium current in rat isolated hippocampal CA1 pyramidal neurons. *J Pharmacol Exp Ther* 256:169–175.
- Takahashi K, Wakamori M, Akaike N (1989) Hippocampal CA1 pyramidal cells of rats have four voltage-dependent calcium conductances. *Neurosci Lett* 104:229–234.
- Takahashi K, Uno S, Akaike N (1991) Kinetic properties of T-type Ca^{2+} currents in isolated rat hippocampal CA1 pyramidal neurons. *J Neurophysiol* 65:148–155.
- Tang C-M, Presser F, Morad M (1988) Amiloride selectively blocks the low threshold (T) calcium channel. *Science* 240:213–215.
- Trimmer JS, Agnew WS (1989) Molecular diversity of voltage-sensitive Na channels. *Annu Rev Physiol* 51:401–418.
- Tseng G-F, Parada I, Prince DA (1991) Double labelling with rhodamine beads and biocytin: a technique for studying corticospinal and other projection neurons *in vitro*. *J Neurosci Methods* 37:121–131.
- Tsien RW, Hess P, Nilius B (1987) Cardiac calcium currents at the level of single channels. *Experientia* 43:1169–1172.
- Yellen G (1982) Single Ca^{2+} -activated nonselective cation channels in neuroblastoma. *Nature* 296:357–359.
- Yoshii M, Tsunoo A, Narashashi T (1988) Gating and permeation properties of two types of calcium channels in neuroblastoma cells. *Biophys J* 54:885–895.